Numerical study of the error sources in the experimental estimation of thermal diffusivity: an application to debris-covered glaciers

Calvin Beck[1,2] and Lindsey Nicholson[2]

[1]Normandie Université – UNICAEN - UNIROUEN, CNRS, UMR 6143 M2C, Laboratoire Morphodynamique Continentale et Côtière, Caen, France
[2]Department of Atmospheric and Cryospheric Sciences, University of Innsbruck, Innsbruck, Austria

Correspondence: Calvin Beck (calvin.beck@unicaen.fr)

Abstract.

In tectonically active mountain regions, the thinning of alpine glaciers due to climate change favors the development of debris covered glaciers. This debris layer significantly modifies a glacier's melt depending on the debris thickness and therefore modifies its evolution. Debris thermal conductivity is a critical parameter for calculating ice melt beneath a debris layer. The most commonly used method to calculate apparent thermal conductivity of supraglacial debris layers is based on an estimate of volumetric heat capacity of the debris and simple heat diffusion principles presented by Conway and Rasmussen (2000). The analysis of heat diffusion requires a vertical array of temperature measurements through the supraglacial debris cover. This study explores the effect of the temporal and spatial sampling interval, and method on the thermal diffusivity values derived using this method. Results show that increasing temporal and spatial sampling intervals increase truncation errors and therefore systematically underestimate values of thermal diffusivity. Also, the thermistor precision, the shape of the diurnal temperature cycle, and vertical thermistor displacement result in systematic errors. Overall these systematic errors would result in an underestimation of glacier ice melt under a debris layer. We have developed a best practice guideline to help other researchers to investigate the effect of the sampling interval on their calculated sub-debris ice melt and better plan future measurement campaigns.

1 Introduction

A glacier's response to climate forcing is drastically modified by its debris cover (Østrem, 1959; Rowan et al., 2015; Huo et al., 2021; Mayer and Licciulli, 2021; Nicholson et al., 2021). However, debris cover has only recently been incorporated into global scale glacier models (Rounce et al., 2015) because it was previously assumed to affect only a relatively small part of the glacier (Hock et al., 2019). Newer studies (Herreid and Pellicciotti, 2020) show that $7.3 \pm 3.3\%$ of all mountain-glacier area is covered by a rock debris cover. This value is likely to increase in the future as global studies conclusively show that a glacier retreat and thinning due to a warming climate results in a debris layer thickening and increase in surface area (Deline and Orombelli, 2005; Kellerer-Pirklbauer et al., 2008; Quincey and Glasser, 2009; Bhambri et al., 2011; Bolch et al., 2012; Kirkbride and Deline, 2013; Thakuri et al., 2014; Scherler et al., 2018; Tielidze et al., 2020). Therefore, the impact of these debris-covered areas will become even more relevant in the future.

25   Most of these debris-covered glaciers occur in tectonically active mountain regions such as Alaska, the European Alps, High Mountain Asia, or New Zealand (Herreid and Pellicciotti, 2020). Here, large amounts of debris migrate into the ice through glacial and periglacial processes (Shugar and Clague, 2011; Scherler et al., 2018; Anderson et al., 2018). This debris is transported englacially to the ablation area of the glacier, where it melts to the surface and forms a supraglacial debris cover or thickens the existing layer (Nicholson and Benn, 2006; Kirkbride and Deline, 2013; Anderson et al., 2018), as shown in Figure
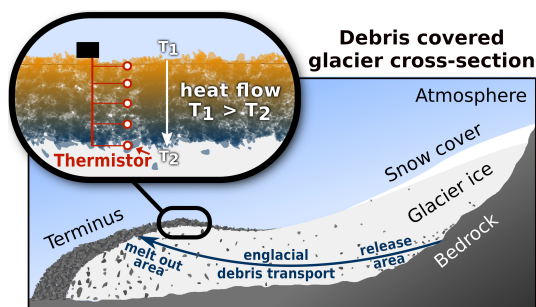
30   1.

Figure 1. Scheme of a debris-covered glacier with debris transport due to bed-rock erosion from release area to melt out area. Zoom of thermal diffusivity measurement site, consisting of thermistors at several heights between the near-surface and the debris-ice interface.

In comparison to clean ice, the debris layer strongly modulates the glacier's melt. Below a certain critical debris thickness or where debris is patchy, ice melt is amplified due to its higher absorptivity of short-wave radiation in comparison to clean ice. On the other hand, thicker debris layers reduce ice melt due to the insulation and attenuation of the diurnal heating signal (Inoue and Yoshida, 1980; Kayastha et al., 2000; Kirkbride and Dugmore, 2003; Mihalcea et al., 2006; Brock et al., 2010;

35   Fyffe et al., 2014; Minora et al., 2015). This debris-depth-dependent ablation rate varies for different debris layer compositions and prevailing climatological conditions but retains the same character (Fig. 2).

The critical debris thickness beyond which sub-debris ice ablation is inhibited compared to clean ice ablation ranges from 15 to 115 mm (Østrem, 1959; Mattson, 1993; Nicholson and Benn, 2006). The specific value depends on the optical and thermal properties of the debris such as lithology type, size, and color, as well as latitude and elevation and the prevailing meteorological

40   conditions (Inoue and Yoshida, 1980; Nakawo and Takahashi, 1982; Adhikary and Miyazaki, 1997; Reznichenko et al., 2010). Therefore in contrast to clean ice glaciers, where the melt is most significant at low elevations towards the glacier tongue, the melt of debris-covered glaciers depends more on the debris depth than on the elevation (Shah et al., 2019). The diurnal energy cycle creates a thermal imbalance within the debris layer, making estimations of sub-debris ice melt difficult on sub-diurnal timescales (Reznichenko et al., 2010; Nicholson and Benn, 2012). This thermal instability can be seen in vertical temperature

45   profiles with a non-linear temperature gradient due to the prevailing meteorological conditions (Conway and Rasmussen, 2000; Reid and Brock, 2010; Foster et al., 2012; Rounce et al., 2015)). The supply of melt energy to the underlying ice is dependent on the heat transfer through the debris cover, which, although it can occur by several processes is usually represented as an apparent thermal conductivity. The method presented by Conway and Rasmussen (2000) is widely used in publications to
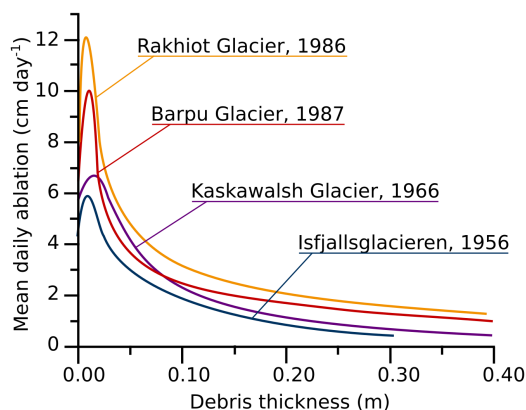
Figure 2. Comparing different measurements of the so-called Østrem curves for different glaciers by displaying the daily melt rate versus the debris depth. The figure is redrawn from Mattson (1993).

calculate the apparent thermal conductivity of supraglacial debris layers (e.g.: Nicholson and Benn, 2006; Haidong et al., 2006; Rounce et al., 2015). It is based on an estimate of the volumetric heat capacity of the debris and simple heat diffusion principles. The analysis of heat diffusion requires a vertical array of temperature measurements (thermistors) through the supraglacial debris cover (Fig. 1). The existing, and limited, sets of field data are used to provide generalized values for the effective thermal conductivity of unmeasured glacier sites and to compare between sites. However, the parameters for temporal or spatial sampling intervals, thermistor spacings, and debris depths used in the application of the standard method presented by Conway and Rasmussen (2000) are selected ad hoc and differ from measurement site to measurement site (e.g. Juen et al., 2013; Chand and Kayastha, 2018; Rowan et al., 2021). Few publications report a robust uncertainty estimate alongside the derived thermal conductivities. This study explores the effect of the chosen temporal and spatial temperature sampling interval and other systematic measurement errors originating in the measurement setup on the derived thermal diffusivity values. Artificially generated data is used to estimate the significance of each of the possible error sources. We present an online tool to explore these errors interactively and a best practice guideline on how to minimize the systematic errors inherent in the standard methods of Conway and Rasmussen (2000).

2   Methods

Thermal conduction describes the flux of thermal energy within or between solids, liquids, or gases due to a temperature gradient (e.g., Borgnakke and Sonntag, 2020). Thermal conductivity k is therefore the material property that describes how quickly a material conducts thermal energy. While conducting energy the material also takes up thermal energy at a certain rate which is called the heat capacity c. This value is calculated by multiplying the specific heat capacity c_s with the material density ρ. Because we can not directly measure a glacier's debris layers thermal conductivity we estimate the thermal diffusivity κ instead (e.g., Salazar, 2003), which is the ratio of thermal conductivity and heat capacity.

$$\kappa = \frac{k}{\rho \cdot c_s} \quad \begin{array}{l} \leftarrow \text{ thermal conductivity} \\ \leftarrow \text{ heat capacity} \end{array} \tag{1}$$

Based on Fourier's law of conduction $q = -k\nabla T$, the one-dimensional heat conduction equation for a homogeneous, isotropic medium can be derived (Fourier, 1955; Cannon, 1984). Here q represents the local heat flux density, k the thermal conductivity, and T the temperature.

$$\frac{\partial T}{\partial t} = \kappa \frac{\partial^2 T}{\partial x^2} \tag{2}$$

While supraglacial debris is not homogeneous and non conductive processes could also contribute to heat transfer, previous research showing linear mean multi-day temperature profiles suggest that the application of 2 to supraglacial debris is generally justifiable (Conway and Rasmussen, 2000; Rowan et al., 2021). The heat equation allows us to calculate the thermal diffusivity given a known temporal temperature gradient and a known second derivative of temperature with respect to space (Bozhinskiy et al., 1986). We follow the approach by Conway and Rasmussen (2000), which has become a standard method for this task (e.g., Nicholson and Benn, 2006; Juen et al., 2013; Chand and Kayastha, 2018; Rowan et al., 2021; Laha et al., 2022). This approach requires a temperature time series from the debris layer with a vertical array of thermistors (Fig 1). From this, the discrete temporal and spatial derivatives of the heat conduction equation can be calculated individually (see section 2.1). We use statistical analysis (see section 2.2) to estimate the value of "apparent" thermal diffusivity κ (Conway and Rasmussen, 2000) assuming a constant density and specific heat capacity. This value is only apparent since one assumes that all energy transfer is by conduction, though subsequently, we will refer to it as thermal diffusivity for simplicity. To explore the capabilities and limitations of this approach we apply this method to artificially generated data with a known value of thermal diffusivity (2.4), which allows us to individually quantify systematic and statistical errors by error source.

In some cases, analysis of field data to determine apparent thermal diffusivity at several levels within the debris cover, rather than as a bulk analysis over all depths, reveals vertical variation in thermal conditions, consistent with stratification of grain size and water content observed in natural debris covers and/or non-conductive processes (Conway and Rasmussen, 2000; Nicholson and Benn, 2012; Petersen et al., 2022). This additional complexity has been addressed in some model studies of energy flux through debris cover that allow, for example, stratification of moisture content Collier et al. (2014); Evatt et al. (2015); Giese et al. (2020). Related inhomogeneity of thermal properties in the debris cover has been accommodated in expansions of the heat equation For example,Laha et al. (2022) perform multiple rather than single regression analysis to account for unknown depth variation in thermal diffusivity in a two-layer model and non-conductive heat sources/sinks. Similarly, Petersen et al. (2022) also included a term for depth varying thermal diffusivity into the heat conduction equation and perform multiple linear regression to solve for thermal diffusivity and its variation with depth in natural debris cover, identifying non-conductive processes as the residual from a comparison of the observed and modelled time dependent temperature evolution. Laha et al. (2022) compare the method of Conway and Rasmussen (2000), to their newly introduced Bayesian inversion method of determining debris thermal properties, for both homogenous and prescribed two-layer debris properties. For the homogenous debris

100 case they highlight the importance of equal vertical spacings between thermistors to reduce truncation errors, and show that if unequal spacing cannot be avoided, the Bayesian method outperforms that of Conway and Rasmussen (2000). As expected, for the two layer debris case they demonstrate that the model versions accommodating this structure outperform model versions forced to solve for a single layer. They limit their multi-layer analysis to the case of three data points within the debris layer and explore the impact of the sampled spacing and ratio of thermal diffusivity above and below the central point. Based on

105 theory and the analysis presented in these two papers, the new or modified methods appear to offer advances on the method of Conway and Rasmussen (2000), but further analysis with a wider selection of datasets would help establish the robustness of the improvement. In this work, we nevertheless focus our analysis on the method of Conway and Rasmussen, as this has been most widely applied in the literature, and understanding the sources of error allows a survey of the likely cross comparability of various debris thermal conductivity values published in the literature. Furthermore, for equally spaced sampling in homoge-

110 nous debris layers, as in our experiments in this study, it has been shown to perform as well as the alternatives (e.g. Laha et al., 2022).

2.1 Numerical approximation

Since our measurement involves discrete values in time and space, we must apply a finite difference method to the one-dimensional heat equation (eq. 2). Therefore we use a second-order accurate central differencing scheme (e.g., Strikwerda,

115 2004). This second order accurate scheme optimizes the differential approximation for the central of three gridpoints. The partial derivative for an arbitrary function $f(n)$ towards a dependency n can be written as follows:

$$\frac{\partial f(n)}{\partial n} \approx \frac{f(n+h) - f(n-h)}{2h} + \mathcal{O}(n^2) \qquad (3)$$

This equation is only valid for equal grid spacing h. If we apply this scheme to the derivatives in the 1D heat equation (eq. 2), we get the following two equations:

$$120 \quad \frac{\partial T_i^n}{\partial t} \approx \frac{T_n^{i+1} - T_n^{i-1}}{2\Delta t} + O(t^2) \qquad (4)$$

$$\frac{\partial^2 T_i^n}{\partial x^2} \approx \frac{T_{i+1}^n - 2T_i^n + T_{i-1}^n}{\Delta x^2} + O(x^2) \qquad (5)$$

Field measurement sites often do not have equal thermistor spacings, so the second spatial derivative has to be transformed to unequal grid spacings described by Sundqvist and Veronis (1970). Numerical approximation schemes result in truncation error, such as using the central difference scheme with second-order accuracy. Truncation errors are expected to scale with

125 the temporal and spatial increment of the analysis with respect to the diurnal forcing cycle Laha et al. (2022). Higher-order approximations would reduce the truncation error, but errors due to measurement uncertainties would dominate, as described by Zhang and Osterkamp (1995). In the analysis in this paper, we will analyze the effects of the combined truncation errors of the spatial and temporal derivatives.

2.2 Statistical analysis

130 Except for the boundary values, we obtain a value for the temporal temperature gradient and the second spatial derivative for each grid point. We plot these two values separately on the x-axis and y-axis and see a correlation for good measurement data. This correlation becomes even better if we consider only calculated values for one height in the debris layer.

Due to the one-dimensional heat equation, we expect a linear correlation between both derivatives. Therefore, we fit a simple linear regression to the data with only the two parameters slope and y-axis intercept (Weisberg (2005)).

$$\frac{\partial T}{\partial t} = \kappa \frac{\partial^2 T}{\partial x^2} + const. \tag{6}$$

135

Here, the value for the slope corresponds to the value of the thermal diffusivity κ, and the intercept accounts in part for the thermistor's systematic temperature error (Conway and Rasmussen (2000)), which is why we can neglect these in our error analysis. To obtain the best linear fit, we use the least-squares method (e.g. Lawson and Hanson, 1995). We look for the fit that minimizes the sum of the distance squares (residuals) between the linear fit function and the measured data.

140 ## 2.3 Measurement uncertainty

To estimate the magnitude of statistical measurement uncertainties relative to the calculated value, we use propagation of uncertainty based on the centered difference scheme equations (Ku et al., 1966). We identify the error in the thermistor temperature accuracy and the vertical spacing in the debris as the two primary measurement-related uncertainty sources in the thermal heat equation. The uncertainty on the distance between thermistors can be calculated using the single uncertainties of the vertical

145 spacings. Since the errors in vertical spacing of each thermistor are assumed to be equal we get the following equation:

$$h = \frac{x_{i+1} - x_{i-1}}{2} \quad \rightarrow \quad \sigma_h = \sqrt{2} \cdot \sigma_x \tag{7}$$

The timing is assumed to be error-free because its accuracy is numerous orders of magnitude smaller than the set point. We then receive the following errors σ on the respective derivative for the equal grid spacing case.

$$\sigma_{\frac{\partial T}{\partial t}} = \frac{\sigma_T}{\sqrt{2}\Delta t} \tag{8}$$

150 $$\sigma_{\frac{\partial^2 T}{\partial x^2}} = \sqrt{\frac{6\sigma_T^2}{h^4} + 4 \cdot \sigma_h^2 \left(T_{i-1}^n - 2T_i^n + T_{i+1}^n \right)} \tag{9}$$

In the analysis, the magnitude of the calculated measurement uncertainties on the derivatives will be compared to the calculated derivative values themselves.

2.4 Artificial data

To test the method by Conway and Rasmussen (2000) for different scenarios, we need to generate artificial measurement

155 data with a known thermal diffusivity value. We use the method by Crank and Nicolson (1947) to solve the heat conduction equation. This implicit finite difference method is convergent second-order in time and numerically stable. The method is based on the trapezoidal rule and is a combination of the Euler forward and backward methods in time. For the thermal heat equation, it results in the following equations:

$$\frac{T_i^{n+1} - T_i^n}{\Delta t} = \frac{\kappa}{\Delta x^2}(T_{i+1}^{n+1} - 2T_i^{n+1} + T_{i-1}^{n+1}) \quad \text{(forward Euler)} \tag{10}$$

160
$$\frac{T_i^{n+1} - T_i^n}{\Delta t} = \frac{\kappa}{\Delta x^2}(T_{i+1}^n - 2T_i^n + T_{i-1}^n) \quad \text{(backward Euler)} \tag{11}$$

Combining the previous two schemes result in the Crank-Nicolson Scheme:

$$\frac{T_i^{n+1} - T_i^n}{\Delta t} = \frac{\kappa}{2\Delta x^2}((T_{i+1}^{n+1} - 2T_i^{n+1} + T_{i-1}^{n+1}) + (T_{i+1}^n - 2T_i^n + T_{i-1}^n)) \quad \text{(Crank-Nicolson)} \tag{12}$$

Because of the implicit nature of the Crank-Nicolson scheme, an algebraic equation or linearizing the equation is necessary to solve the next time step. In the case of our model, we can use the boundary conditions $T(x = 0, t) = f(t)$ and $T(x = D, t) = 0$.

165 Here $f(t)$ represents an arbitrary temperature forcing function (3). Although the method is unconditionally numerically stable for the heat equation (Thomas, 2013), unwanted spurious oscillations can occur if the time steps are too long or the spatial resolution is too small. To avoid this, von Neumann stability conditions must be fullfilled (Charney et al., 1950):

$$\kappa \frac{dt}{dx^2} \leq \frac{1}{2} \tag{13}$$

2.5 Data generation forcing and parameters:

170 To numerically model representative scenarios for a glacier's debris layer we have to select several parameters. For instance we can change the depth of the debris layer by increasing the number of vertical grid points given a constant spatial resolution. Also, the spatial boundary conditions have to be defined. The boundary conditions at the debris-ice interface are set to zero as we assume ice to be at its melting temperature.

For the surface, we use diurnal temperature signals and then force the second boundary condition. We used a sinusoidal

175 daily cycle of each 10 days to represent the most ideal case, then a skewed cycle, and then we forced the model with different types of actual measurement data from within the debris. The first two days of temperature forcing data are used to initialize the model. The color scheme of these forcings will be used throughout this paper to indicate the corresponding forcing.
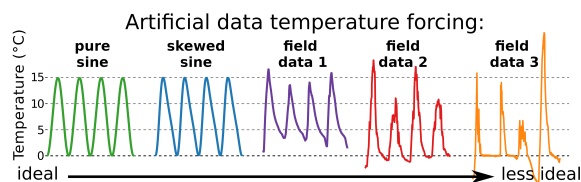
Figure 3. Selected temperature forcings for surface layer consisting of two analytical sine curves and three experimental temperature measurements within the debris layer. The sine curves have a average temperature of $7.5\,°C$ and the same amplitude. Experimental data 3 and 5 was recorded at Lirung glacier (Nepal) during September 2013 (@5cm) and April 2014 (@1cm) respectively and was by provided by Chand and Kayastha (2018). Experimental data 4 was recorded at Vernagtferner (Austria) during June 2010 (@4cm) and was provided by Juen et al. (2013).

For the value of thermal diffusivity, we investigate values of $5 \cdot 10^{-7}\,m^2\,s^{-1}$, and $10 \cdot 10^{-7}\,m^2\,s^{-1}$, because this is a representative range of values obtained from field data (Laha et al., 2022). With these parameters, we execute the Crank-Nicolson
180 scheme to generate the artificial data (see section 2.4).

Here, we display two examples of the generated data as a shortened time series as well as the debris layers' mean daily temperature function. We forced the model by the pure sine curve as well as for experimental data 3 with both a debris depth of $30\,cm$ and thermal diffusivity of $5 \cdot 10^{-7}\,m^2\,s^{-1}$.
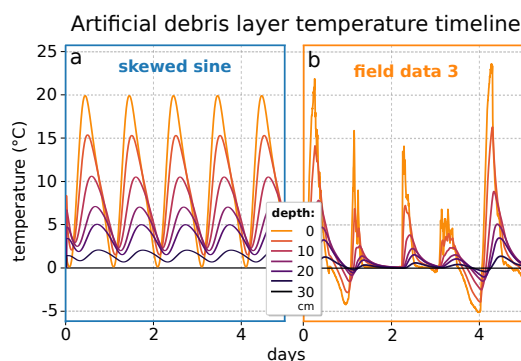

Figure 4. Artificially generated debris layer temperature timeseries data for the skewed sine forcing (a) and the field data 3 foricing (b) for a 30 cm debris layer and thermal diffusivity of $5 \cdot 10^{-7}\,m^2\,s^{-1}$ using Crank-Nicolson scheme.

From Figure 6 we can see that the often-used steady-state assumption (Evatt et al., 2015) of the daily mean debris layer
185 temperature is only fulfilled for perfectly idealized datasets. A glacier's debris layer is at a steady state when the debris layer's temperature decreases linearly towards the debris-ice interface.

In the model, we can also select and de-selected errors and uncertainties to investigate their effect. To account for the fact that measurement devices do not have a double float accuracy as does our model, we can discretize the data to correspond with the measurement uncertainty of 0.1 to 0.4 °C. This is the uncertainty range of thermistors most commonly used in the field.
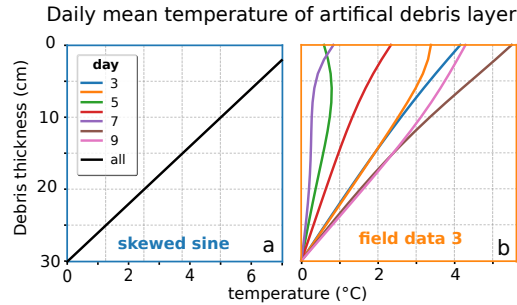
8

Figure 5. Daily averaged debris layer temperature profile based on figure 4.

190 Also, the vertical field deployment of the thermistors is not as exact as in our model. We accounted for that by using a Gaussian random error to displace the values by a Gaussian width of 0.25 and 0.5 centimeters. Additionally, the thermistors may drift over time within the debris layer altering their relative distance.

2.6 Truncation error

The first analysis step is to calculate the truncation error due to the central difference scheme for different temporal and spatial
195 sampling intervals. In theory, the numerical solution should be equal to the analytical solution for infinitesimally small spatial and temporal sampling intervals.

$$\lim_{\Delta t \to 0} \frac{T_{t+1} - T_{t-1}}{2\Delta t} = \dot{T} \qquad \& \qquad \lim_{\Delta t \to 0} \frac{T_{x+1} - T_x + T_{x-1}}{(\Delta x)^2} = T'' \tag{14}$$

For $\Delta x, \Delta t = 0$ the equations are not solvable.

We calculate the relative error as such:

$$\text{Error} = \frac{\kappa_{\text{True}} - \kappa_{\text{Estimated}}}{\kappa_{\text{True}}} \tag{15}$$

Here, positive relative error values in the graph correspond to negative errors in absolute values, therefore underestimating thermal diffusivity values.

2.7 Resampling method

For the temporal resampling, we also compare sampling by skipping and sampling by averaging as displayed in Figure 6. When
205 skipping (method 1), we only select every n-th value and omit the rest. This is the method used by Conway and Rasmussen (2000), and we expect this to be the preferred method since it conserves gradients. The alternative (method 2) is to average over n values. It has the result that gradients are reduced, and therefore the results are expected to be underestimated. To see how this influences the calculations of the thermal diffusivity value, see the next section. A light blue background indicates

sampling by skipping (method 1), and a light orange background indicates sampling by averaging (method 2) is used in the
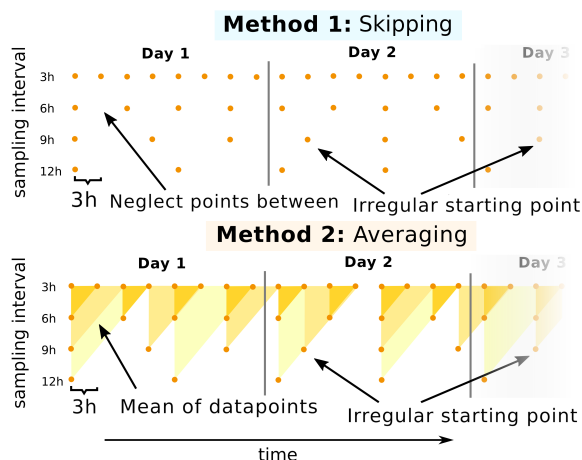following graphics.

Figure 6. Comparing two different temporal resampling methods by displaying the temporal grid for different sampling intervals. We compare the method by skipping every n-th gridpoint (*method 1*) or by averaging over n gridpoints (*method 2*).

3 Results

We start by using the artificial data without any uncertainty added to estimate the temporal truncation error.

3.1 Temporal truncation error

The relative temporal truncation error has a monotonous increasing trend for an increasing sampling time for the skipping
method (Fig. 7a,b).

The exact function is heavily dependent on the forcing type. For less sinusoidal temperature forcings, a more significant
error already occurs at small sampling intervals. All curves collapse on the curve for the pure sinusoidal data at greater depths,
since the greater the depth, the more the diurnal signal approaches a sinusoidal shape. For even larger depths the temporal
truncation error of the experimental data decreases even more. However, at these large depths, the measurement uncertainty
becomes dominant. We will demonstrate this in subsection 3.3 by adding uncertainty to the artificial data. When switching to
the averaging method, the temporal error is already less extreme for the example data but shows similar behavior as for the
skipping method (Fig. 7c, d).

The value for the sine curve is constant over different depths in the debris layer for different temperature forcings. Positive
relative truncation errors due to the temporal sampling interval systematically underestimate values of thermal diffusivity and
therefore systematically underestimate glacier melt. Therefore from a truncation perspective, a minimum temporal resolution
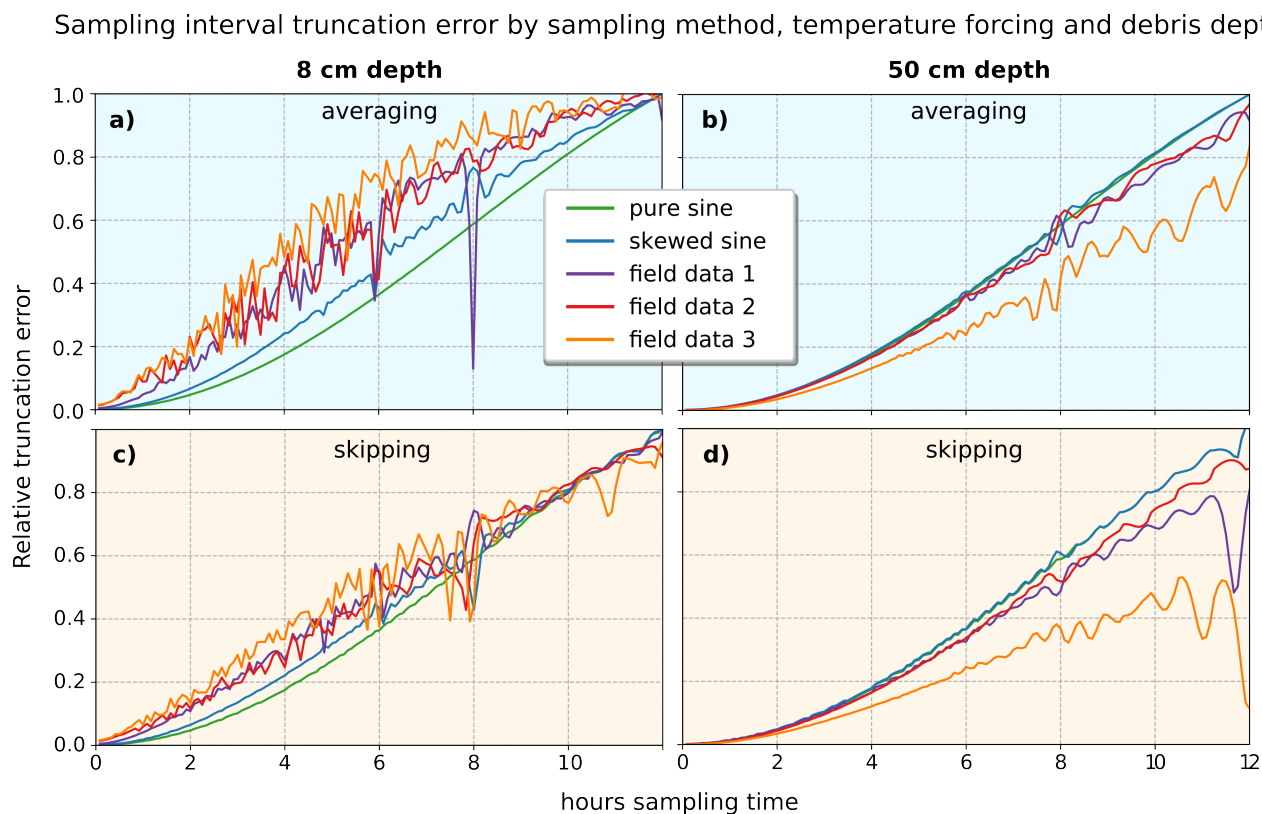is desirable.

10

Figure 7. Relative temporal truncation error of thermal diffusivity estimation by sampling interval. We compare different temperature forcing for averaging (a,b) and skipping (c,d) re-sampling methods for two different depths in the debris layer.

3.2 Spatial truncation error

We now analyze the spatial truncation error again without uncertainties added. Therefore we sample over the spatial grid size with two times Δx displayed on the x-axis and different temporal sampling intervals in minutes displayed in different colors
230 (Fig. 8). Values are constant for low Δx, but the relative error then drastically increases for large Δx. The spatial truncation error does not change with different model forcings or with debris depth. The main critical parameter is the value of thermal diffusivity, because the truncation error increases for smaller values of thermal diffusivity. However, this value is not known beforehand, so a range up to a Δx of 0.1 meters is desirable. This error would systematically underestimate glacier melt.

3.3 Error due to thermistor uncertainty (spatial sampling)

235 Now we look at errors due to the measurement uncertainty to make our model more comparable to real-world data. Therefore we add a temperature discretization from 0.1 to 0.4 °C since these are the discretizations of the thermistors used to create our
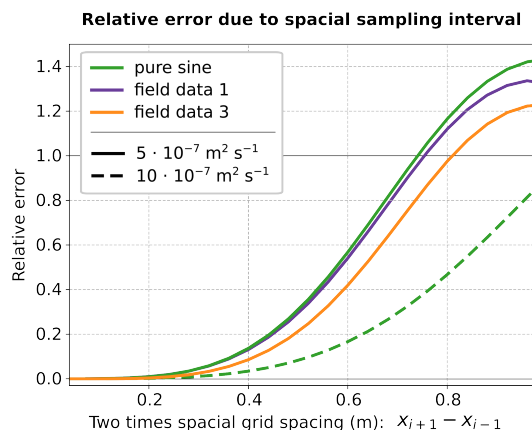
Figure 8. Comparing the spatial truncation error for different thermal diffusivity values and forcing types.

datasets. We again sample over the thermistor spacings but only focus on the region not affected by the truncation error (Fig. 9). Because we added temperature uncertainty, it now makes a difference how we sample the thermistor spacings. One can either start at the top - so from the surface layer - and increase the Δx from there. Alternatively, one starts in the middle of the debris layer and selects Δx symmetrically. The third option is to start at the debris-ice interface and go up from there with increasing measurement uncertainty. For small values of Δx the relative error spikes and exponentially decreases for larger values of Δx. The averaging method produces different but similar results. We see that this error is less pronounced even for lower thermistor uncertainties. Values of Δx between the dominant spatial truncation error and the error due to the uncertainty are desirable, so between 5 and 15 centimeters. This error would systematically underestimate glacier melt.

3.4 Error due to thermistor uncertainty (depth in debris)

As demonstrated in subsection 3.2, the relative error increases with increasing thermistor spacing due to the smaller gradients. We now investigate the depth dependence of constant vertical sampling intervals (Fig. 10).

The different color lines correspond to different values of temperature uncertainty. For a Δx of two centimeters, only measurements with a thermistor uncertainty of $0.1\,°C$ would produce correct values for the first 20 centimeters of debris. Switching to an Δx of 6 centimeters, the relative error decreases for all curves. Still, the thermistors used in the field experiment range from 0.1 to $0.4\,°C$ would not produce correct values. When increasing the sampling time to around 60 minutes, results improve for the layers close to the surface before the temporal truncation error becomes relevant. For higher sampling intervals, the averaging method here performs even better. This shows the importance of high-resolution thermistors even with larger spatial sampling intervals. For deeper debris layers it is not possible to obtain correct values even with high-resolution thermistors.
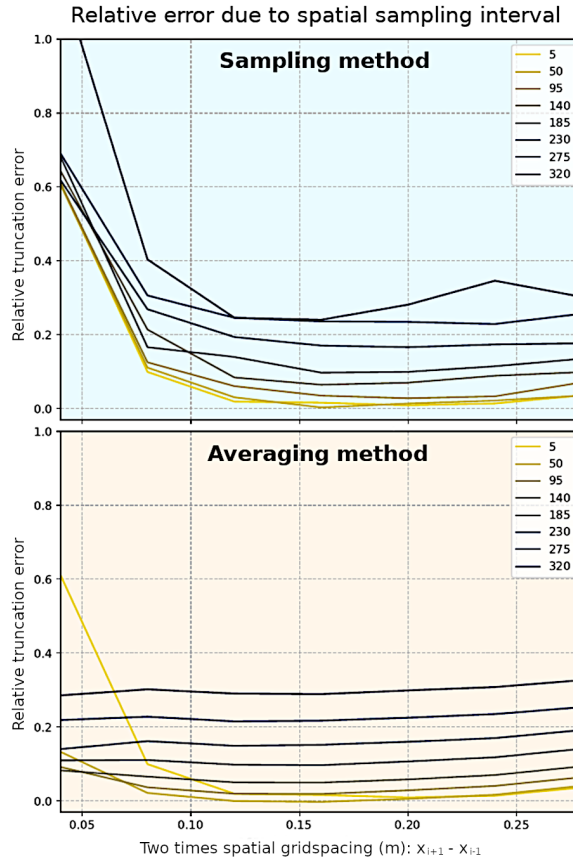
Figure 9. Relative error of estimated thermal diffusivity value due to thermistor temperature discretisation of $0.4°C$ while comparing the sampling and averaging method. Sampled from the surface layer downward.

3.5 Error due to vertical thermistor position variability

Conway and Rasmussen (2000) report that a vertical error of 0.5 cm would result in a marginal temperature difference of $0.1\,\mathrm{K}$ and $0.02\,\mathrm{K}$ for their measurement setups. This is then interpreted by them and others (e.g. Nicholson and Benn, 2012) that a vertical thermistor displacement would not affect the results as long as this value does not change in time. In their derivation they assumed an error ϵ in the depth z, which should correspond to the mean error δ which should then be proportional to the mean vertical temperature gradient:

$$\delta = \epsilon \frac{\partial \bar{T}}{\partial z} \tag{16}$$

By averaging over the temperature, the temporal dependency is neglected. However, we are not interested in temperature errors but the errors in the gradients, which are time-dependent.
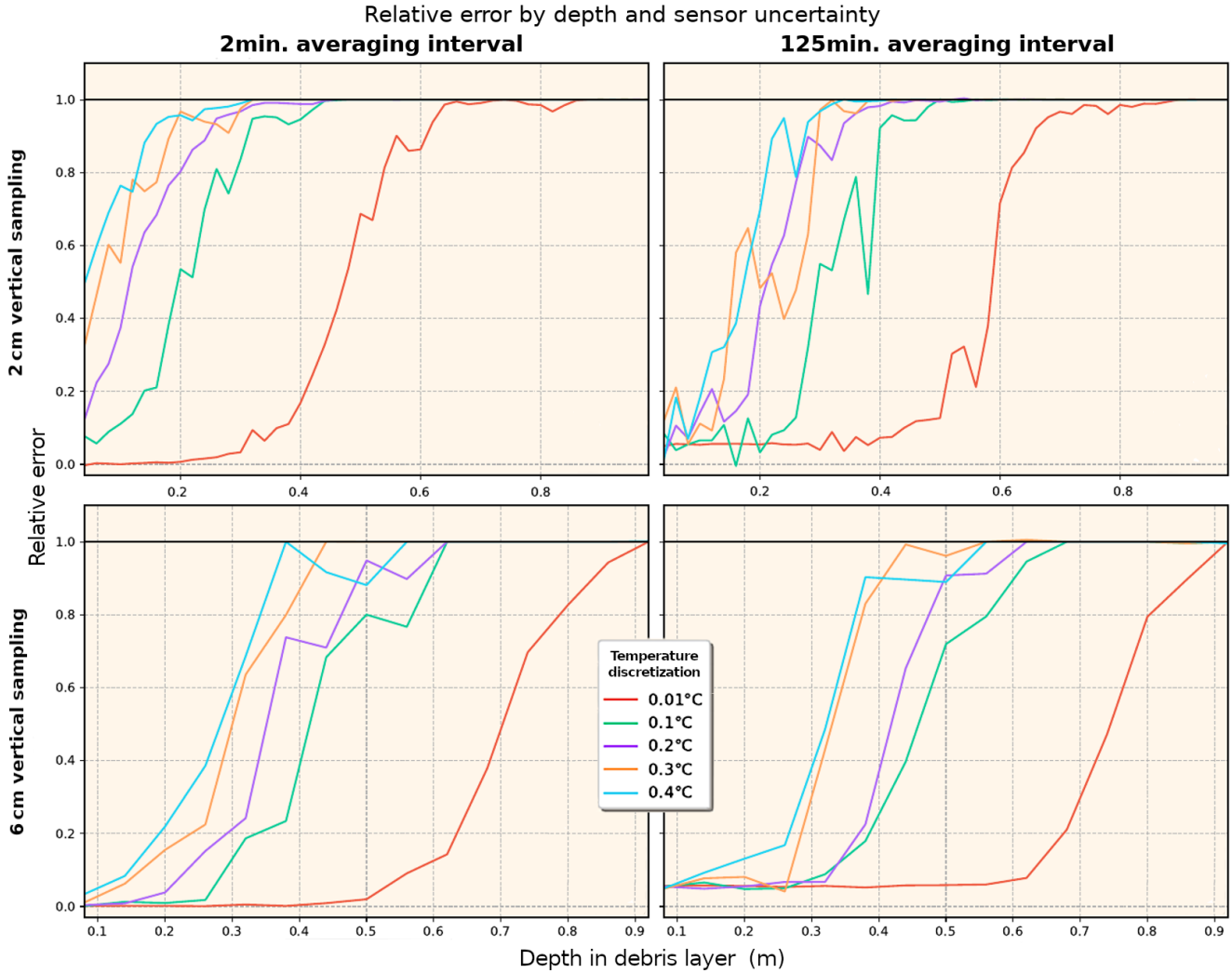
13

Figure 10. Relative error of estimated thermal diffusivity value due to thermistor discretization by depth in the debris up to 0.9 m.

We use a similar approach as Conway and Rasmussen with equation 16 without averaging over the vertical temperature
gradient and define this as the temperature error due to the vertical displacement of the thermistor. If we add this error to the
true temperature we get the measured temperature Θ:

$$\Theta(t) = T(t) + \delta(t), \quad with \quad \delta(t) = \epsilon \frac{\partial T(t)}{\partial z} \tag{17}$$

If we insert this equation into the heat equation (Eq. 2) we get the following equation:

$$\frac{\partial T}{\partial t} + \frac{\partial \delta}{\partial t} = \kappa \frac{\partial^2 T}{\partial x^2} + \kappa \frac{\partial^2 \delta}{\partial x^2} \tag{18}$$
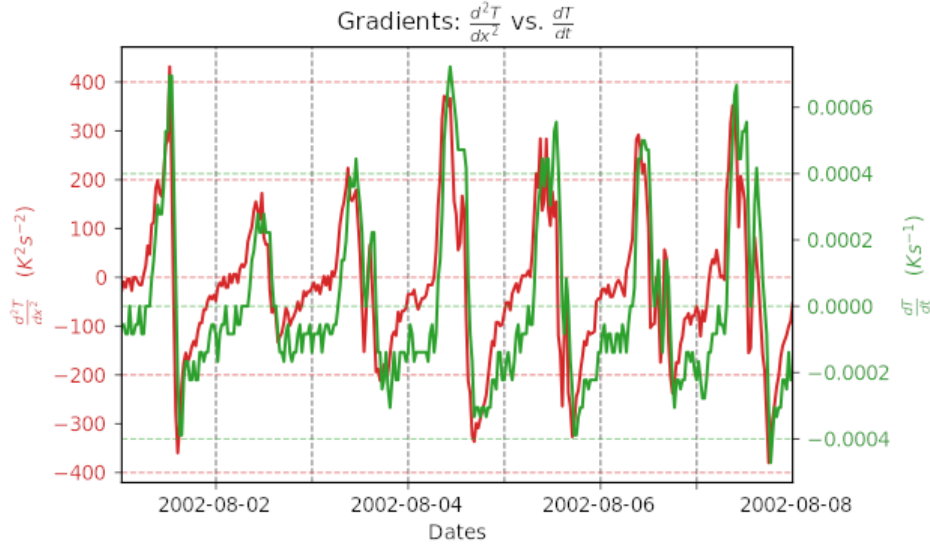
EGUsphere
Preprint repository

Figure 11. Timeseries of temporal gradient and second spatial derivative of Ngozumpa glacier debris layer temperature data-set (Nicholson and Benn, 2006)

270   Since δ is time-dependent, it does not vanish in the constant Y-intercept term during the linear regression. A better method of visualizing the error due to a vertical thermistor displacement is not to argue over an altered temperature, but instead of an error in the distance between thermistors $\delta x + \delta \epsilon$. In this case, there is no error on the temporal gradients and we can purly focus on the spatial derivative. For simplicity, we use the equal grid centered difference scheme equation for the second spatial derivative (Eq. 5) and add the error $\Delta \epsilon$:

$$275 \quad \frac{\partial^2 T_i^n}{\partial x^2} \approx \frac{T_{i+1}^n - 2T_i^n + T_{i-1}^n}{(\Delta x + \Delta \epsilon)^2} + O(x^2) \tag{19}$$

To get the relative error, we then divide the true derivative by the derivative with the added error:

$$\text{Relative error} = \frac{\Delta x^2}{(\Delta x + \Delta \epsilon)^2} = 1 + \frac{\Delta \epsilon}{\Delta x} + \frac{\Delta \epsilon^2}{\Delta x^2} \tag{20}$$

Based on this equation, we can see that the relative error of the derivative depends not only on the displacement error but also on the distance between the two thermistors.

280   We now plot this equation for different errors and Δx combinations:

It is clear that the larger the distance between thermistors, the smaller the relative error becomes, and the larger $\Delta \epsilon$, the more the error increases. However, since this is just the relative error on the second spatial derivative, it is not yet that meaningful. Therefore next, we simulate the vertical displacement of a thermistor (Fig. 13). Therefore we set the temperature uncertainty back to zero and add a gaussian uncertainty on the vertical thermistor position of 0.25 and 0.5 centimeters. In reality, for
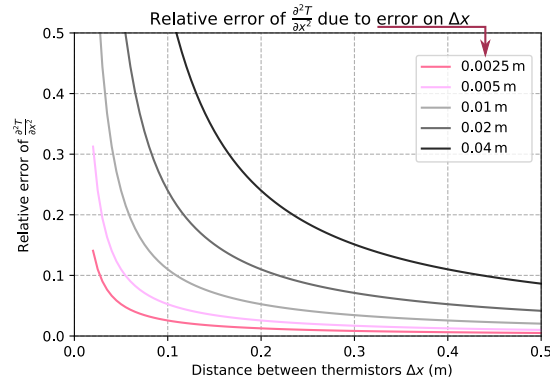
15

Figure 12. Relative error on second spatial derivative due to different values of displacement errors on Δx.
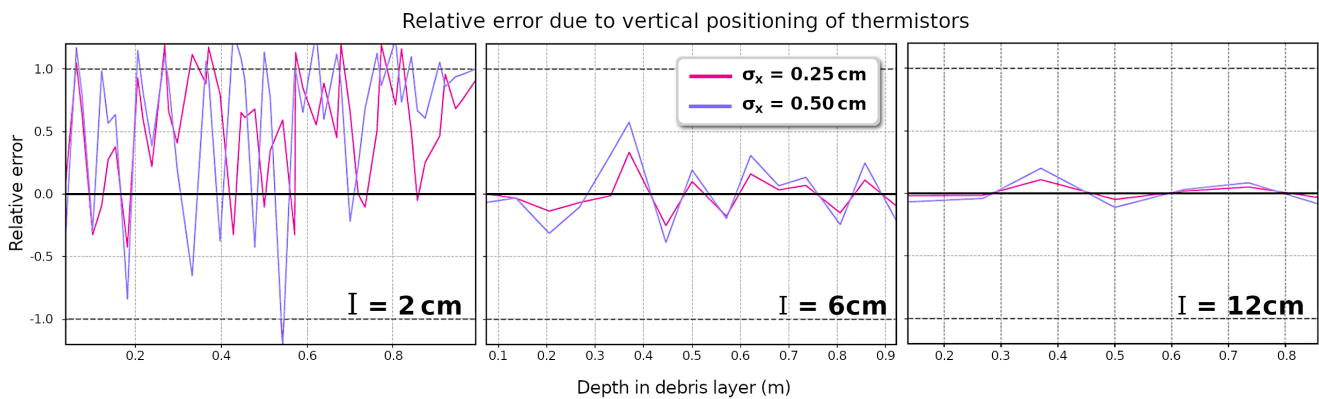

Figure 13. Relative error on debris thermal diffusivity value due to vertical thermistor displacement. The thermistors are randomly displaced with a normal distribution with standard deviation $0.25\,\mathrm{cm}$ and $0.5\,\mathrm{cm}$ for different spatial thermistor sampling intervals I of $2\,\mathrm{cm}$, $6\,\mathrm{cm}$, and $12\,\mathrm{cm}$ respectively.

285   moving thermistors in the debris layer, the value can even be larger. For an Δx of two centimeters, the data would be completely unusable. This error source is the only one in the complete analysis that has the potential to increase thermal diffusivity values shown here by the negative relative error values. As expected, with increasing Δx, the relative error decreases until a distance is reached where the the spatial truncation error becomes relevant again (see section 3.2).

4   Discussion

290   Conway and Rasmussen (2000) provide a simple and easy to apply method to estimate thermal diffusivity values from a vertical array of thermistors in the debris layer. Therefore this method has developed to be the standard method for this task (e.g. Nicholson and Benn, 2006; Juen et al., 2013; Nicholson and Benn, 2012; Rounce et al., 2015; Chand and Kayastha, 2018;

Rowan et al., 2021). However, it is regularly used without considering possible limitations or error sources. Here, we have shown how careful one has to be during the analysis of the data using this method and how relevant an appropriate experimental setup is. Truncation errors, errors due to measurement uncertainty, or the impact of non-conductive processes are often not sufficiently taken into account in the uncertainty estimation of the above mentioned publications. In general, all truncation errors and errors due to measurement uncertainties systematically underestimate thermal diffusivity values. Too large temporal or spatial sampling intervals both result in non-linear significant truncation errors. Especially near-surface measurements are problematic because the diurnal temperature cycle is most non-sinusoidal within the debris layer and therefore produces more significant temporal truncation errors. On the other hand, sinusoidal temperature cycles produce the least truncation error in the analysis and are preferred. The deeper the debris layer, the more the temperature cycle smoothens out and becomes more sinusoidal. Even though a Δt or $\Delta x \longrightarrow 0$ would produce a minimal truncation error, too small sampling intervals also can produce erroneous results. For a $\Delta t \longrightarrow 0$, the linear regressions coefficient of determination decreases strongly. In practice, this is not a problem since short temporal sampling intervals can always be resampled afterwards. A more significant problem is if thermistors are positioned too close to each other, especially if there are only a few thermistors, making it impossible to spatially resample. Here the thermistor discretization results in underestimated values of thermal diffusivity. Also, with increasing depth, the thermistors in the debris layer have to be positioned at greater distances from each other because otherwise, the thermistor measurement uncertainty dominates the measurement. Therefore, at greater depths in the debris layer, it is not wise to perform measurements unless very precise measuring instruments are available $\leq 0.01\,\mathrm{K}$. The only error source due to the measurement setup that has the potential to overestimate the thermal diffusivity value is the vertical displacement of the thermistors. In contrast to the derivation by Conway and Rasmussen (2000), the calculated value of thermal diffusivity strongly depends on correct thermistor positions relative to each other. Comparing our findings to the recommendations of Laha et al. (2022), they propose to "set the sensor spacing to be $1/5^{th}$ of the debris thickness at the location", however the non-linear nature of the single error sources presented in this paper indicates that we cannot generalize such statements. Furthermore, they stated "the top sensor should be placed approximately at the middle of the debris layer" and our analysis indicates that while it is true, that thermistors too close to the surface produce large truncation errors, the same is valid for too deep thermistors as the temperature gradient is to small relative to the thermistor precision. Finally, in addition to all these measurement setup related errors, non-conductive processes within the debris layer (e.g. rain, phase changes) would distort the results. This must be evaluated on a case-by-case basis using meteorological data and closely evaluating the vertical temperature measurements in the debris layer and the corresponding gradient functions Petersen et al. (2022). All of this makes it challenging to interpret the results correctly leaving considerable room for error, especially since the datasets often lack relevant meta- and meteorological data. This has to be better reflected in the published measurement uncertainty.

The following best practice guidelines address all sources of error discussed in this paper and are the basis for producing more reliable measurement data and therefore values of thermal diffusivity. With this we aim to provide an implementation strategy for future field studies that wish to deploy these methods of analysing the thermal conductivity of natural debris layers. We provide an open source program where researchers can modify the single parameters to their needs and therefore can also

17

investigate the chances and limitations of applying the method by Conway and Rasmussen (2000) to other regimes outside of glaciology.

5   Best practice guidelines

330   When working in the field on a glacier, things do not always go as planned in the warm office. Therefore, it is even more essential to develop a precise concept for the measurement beforehand, which can then be worked through step by step in the field. In addition to the recommendations put forward in Laha et al. (2022) our analysis leads us to the following best practice guidelines to help other researchers to get as much as possible out of their measurements.

335

Thermistor precision:

As small as possible, but not larger than 0.1 K.

Debris layer depth:

Minimum of 40 cm but ideally deeper (e.g. 100 cm). The maximum depth is limited by the thermistor precision and temperature gradients in the debris layer. This can be simulated beforehand.

Thermistor installation and recovery:

Thermistors have to be carefully extracted at the end of the measurement period to make sure the thermistors haven't moved in the debris while deployed. However, in case the thermistors moved, it might be necessary to omit this dataset. Therefore mounting thermistors to a thermally insulated rod or set of rods eliminates this potential error source.

Number of thermistors:

The method requires at least three thermistors, but more thermistors make it possible to calculate diffusivity values for different depths and therefore makes it possible to identify non-conductive processes or other inconsistencies. A second redundant set of thermistors can also be helpful to rule out measurement errors.

Thermistor arrangement:

Place thermistors at equal vertical intervals of 8 to 20 cm. Even though the upper-most layer often does not produce ideal results, it can be helpful to place a thermistor at the debris-ice interface still because, this way, the debris layer can subsequently be simulated. Depending on the depth, the thermal diffusivity, and gradient of the debris layer, the method produces more significant errors with a greater depth limiting the depth where it makes sense to place thermistors. The sweet spot can be determined by simulating the debris layer of interest beforehand with model parameters from previous measurements or other estimations.

340

Temporal sampling interval:

Sample with a temporal resolution as short as possible and then average over a 5 minute period. Over such a short period, the temperature is assumed to be nearly constant and therefore not to reduce gradients. By averaging the thermistor, discretization is reduced.

Measurement duration:

It depends on the scientific objective and seasonality, but at least a week of suitable stable meteorological conditions are needed. Therefore, if one has unlucky conditions, a measurement duration of several months can be necessary.

Suitable meteorological conditions:

Avoid precipitation, phase changes and aim for a sinusoidal diurnal cycles in the forcing data.

Code availability. Publicly available under: https://github.com/calvinbeck/DTD

345 *Author contributions.* This publication is based on the MSc thesis of CB, supervised by LN. LN conceived the study, CB performed all analysis, developed the online tool, produced the figures and led the preparation of the manuscript. Both CB and LN worked to finalise the manuscript for publication.

Competing interests. The authors declare that they have no conflict of interest.

References

Adhikary, S., K. S. M. N. Y. A. and Miyazaki, N.: Effect of surface dust on snow melt, Bulletin of glacier research, 15, 85–92, 1997.

Anderson, R. S., Anderson, L. S., Armstrong, W. H., Rossi, M. W., and Crump, S. E.: Glaciation of alpine valleys: The glacier–debris-covered

355   glacier–rock glacier continuum, Geomorphology, 311, 127–142, https://doi.org/10.1016/j.geomorph.2018.03.015, 2018.

Bhambri, R., Bolch, T., Chaujar, R. K., and Kulshreshtha, S. C.: Glacier changes in the Garhwal Himalaya, India, from 1968 to 2006 based

    on remote sensing, Journal of Glaciology, 57, 543–556, https://doi.org/10.3189/002214311796905604, 2011.

Bolch, T., Kulkarni, A., Kääb, A., Huggel, C., Paul, F., Cogley, J. G., Frey, H., Kargel, J. S., Fujita, K., and Scheel, M.: The state and fate of

    Himalayan glaciers, Science, 336, 310–314, 2012.

360 Borgnakke, C. and Sonntag, R. E.: Fundamentals of thermodynamics, John Wiley & Sons, 2020.

Bozhinskiy, A., Krass, M., and Popovnin, V.: Role of debris cover in the thermal physics of glaciers, Journal of Glaciology, 32, 255–266,

    https://doi.org/10.3189/S0022143000015598, 1986.

Brock, B. W., Mihalcea, C., Kirkbride, M. P., Diolaiuti, G., Cutler, M. E., and Smiraglia, C.: Meteorology and surface energy fluxes in

    the 2005–2007 ablation seasons at the Miage debris-covered glacier, Mont Blanc Massif, Italian Alps, Journal of Geophysical Research:

365   Atmospheres, 115, https://doi.org/10.1029/2009JD013224, 2010.

Cannon, J. R.: The one-dimensional heat equation, Cambridge University Press, 1984.

Chand, M. B. and Kayastha, R. B.: Study of thermal properties of supraglacial debris and degree-day factors on Lirung Glacier, Nepal,

    SCAR, 10, 357–368, https://doi.org/10.3724/SP.J.1226.2018.00357, 2018.

Charney, J. G., Fjörtoft, R., and Von Neumann, J.: Numerical integration of the barotropic vorticity equation, in: The Atmosphere—A

370   Challenge, pp. 267–284, Springer, https://doi.org/10.1007/978-1-944970-35-2_15, 1950.

Collier, E., Nicholson, L., Brock, B., Maussion, F., Essery, R., and Bush, A.: Representing moisture fluxes and phase changes in glacier

    debris cover using a reservoir approach, The Cryosphere, 8, 1429–1444, 2014.

Conway, H. and Rasmussen, L. A.: Summer temperature profiles within supraglacial debris on Khumbu Glacier, Nepal, IAHS PUBLICA-

    TION, pp. 89–98, 2000.

375 Crank, J. and Nicolson, P.: A practical method for numerical evaluation of solutions of partial differential equations of the heat-conduction

    type, Mathematical Proceedings of the Cambridge Philosophical Society, 43, 50–67, https://doi.org/10.1017/S0305004100023197, 1947.

Deline, P. and Orombelli, G.: Glacier fluctuations in the western Alps during the Neoglacial, as indicated by the Miage morainic amphitheatre

    (Mont Blanc massif, Italy), Boreas, 34, 456–467, https://doi.org/10.1111/j.1502-3885.2005.tb01444.x, 2005.

Evatt, G. W., Abrahams, I. D., Heil, M., Mayer, C., Kingslake, J., Mitchell, S. L., Flowler, A. C., and Clark, C. D.: Glacial melt under a

380   porous debris layer, Journal of Glaciology, 61, 825–836, 2015.

Foster, L., Brock, B., Cutler, M., and Diotri, F.: A physically based method for estimating supraglacial debris thickness from thermal band

    remote-sensing data, Journal of Glaciology, 58, 677–691, https://doi.org/10.3189/2012JoG11J194, 2012.

Fourier, J.-B.-J.: The analytical theory of heat, Courier Corporation, 1955.

Fyffe, C. L., Reid, T. D., Brock, B. W., Kirkbride, M. P., Diolaiuti, G., Smiraglia, C., and Diotri, F.: A distributed energy-balance melt model

385   of an alpine debris-covered glacier, Journal of Glaciology, 60, 587–602, https://doi.org/10.3189/2014JoG13J148, 2014.

Giese, A., Boone, A., Wagnon, P., and Hawley, R.: Incorporating moisture content in surface energy balance modeling of a debris-covered

    glacier, The Cryosphere, 14, 1555–1577, 2020.

Haidong, H., Yongjing, D., and Shiyin, L.: A simple model to estimate ice ablation under a thick debris layer, Journal of Glaciology, 52, 528–536, https://doi.org/10.3189/172756506781828395, 2006.

390 Herreid, S. and Pellicciotti, F.: The state of rock debris covering Earth's glaciers, Nature Geoscience, 13, 621–627, 2020.

Hock, R., Bliss, A., Marzeion, B., Giesen, R. H., Hirabayashi, Y., Huss, M., Radić, V., and Slangen, A. B.: GlacierMIP–A model intercomparison of global-scale glacier mass-balance models and projections, Journal of Glaciology, 65, 453–467, https://doi.org/10.1017/jog.2019.22, 2019.

Huo, D., Bishop, M. P., and Bush, A. B.: Understanding complex debris-covered glaciers: Concepts, issues, and research directions, Frontiers
395   in Earth Science, 9, 652 279, 2021.

Inoue, J. and Yoshida, M.: Ablation and Heat Exchange over the Khumbu Glacier Glaciological Expedition of Nepal, Contribution No. 65 Project Report No. 4 on "Studies on Supraglacial Debris of the Khumbu Glacier", Journal of the Japanese Society of Snow and Ice, 41, 26–33, https://doi.org/10.5331/seppyo.41.Special_26, 1980.

Juen, M., Mayer, C., Lambrecht, A., Wirbel, A., and Kueppers, U.: Thermal properties of a supraglacial debris layer with respect to lithology
400   and grain size, Geografiska Annaler: Series A, Physical Geography, 95, 197–209, https://doi.org/10.1111/geoa.12011, 2013.

Kayastha, R. B., Takeuchi, Y., Nakawo, M., and Ageta, Y.: Practical prediction of ice melting beneath various thickness of debris cover on Khumbu Glacier, Nepal, using a positive degree-day factor, Iahs Publication, 7182, 2000.

Kellerer-Pirklbauer, A., Lieb, G. K., Avian, M., and Gspurning, J.: The response of partially debris-covered valley glaciers to climate change: the example of the Pasterze Glacier (Austria) in the period 1964 to 2006, Geografiska Annaler: Series A, Physical Geography, 90, 269–285,
405   https://doi.org/10.1111/j.1468-0459.2008.00345.x, 2008.

Kirkbride, M. P. and Deline, P.: The formation of supraglacial debris covers by primary dispersal from transverse englacial debris bands, Earth Surface Processes and Landforms, 38, 1779–1792, https://doi.org/10.1002/esp.3416, 2013.

Kirkbride, M. P. and Dugmore, A. J.: Glaciological response to distal tephra fallout from the 1947 eruption of Hekla, south Iceland, Journal of Glaciology, 49, 420–428, https://doi.org/10.3189/172756503781830575, 2003.

410 Ku, H. H. et al.: Notes on the use of propagation of error formulas, Journal of Research of the National Bureau of Standards, 70, 263–273, 1966.

Laha, S., Winter-Billington, A., Banerjee, A., Shankar, R., Nainwal, H. C., and Koppes, M.: Estimation of ice ablation on a debris-covered glacier from vertical debris-temperature profiles, Journal of Glaciology, pp. 1–12, https://doi.org/10.1017/jog.2022.35, 2022.

Lawson, C. L. and Hanson, R. J.: Solving least squares problems, SIAM, 1995.

415 Mattson, L. E.: Ablation on debris covered glaciers: an example from the Rakhiot Glacier, Punjab, Himalaya, Intern. Assoc. Hydrol. Sci., 218, 289–296, 1993.

Mayer, C. and Licciulli, C.: The concept of steady state, cyclicity and debris unloading of debris-covered glaciers, Frontiers in Earth Science, 9, 710 276, 2021.

Mihalcea, C., Mayer, C., Diolaiuti, G., Lambrecht, A., Smiraglia, C., and Tartari, G.: Ice ablation and meteorological conditions on the debris-
420   covered area of Baltoro glacier, Karakoram, Pakistan, Annals of Glaciology, 43, 292–300, https://doi.org/10.3189/172756406781812104, 2006.

Minora, U., Senese, A., Bocchiola, D., Soncini, A., D'agata, C., Ambrosini, R., Mayer, C., Lambrecht, A., Vuillermoz, E., and Smiraglia, C.: A simple model to evaluate ice melt over the ablation area of glaciers in the Central Karakoram National Park, Pakistan, Annals of Glaciology, 56, 202–216, https://doi.org/10.3189/2015AoG70A206, 2015.

425 Nakawo, M. and Takahashi, S.: A simplified model for estimating glacier ablation under a debris layer, IAHS Publ, 138, 137–145, 1982.

Nicholson, L. and Benn, D. I.: Calculating ice melt beneath a debris layer using meteorological data, Journal of Glaciology, 52, 463–470, https://doi.org/10.3189/172756506781828584, 2006.

Nicholson, L. and Benn, D. I.: Properties of natural supraglacial debris in relation to modelling sub-debris ice ablation, Earth Surface Processes and Landforms, 38, 490–501, https://doi.org/10.1002/esp.3299, 2012.

430   Nicholson, L., Wirbel, A., Mayer, C., and Lambrecht, A.: The challenge of non-stationary feedbacks in modeling the response of debris-covered glaciers to climate forcing, Frontiers in Earth Science, 9, 662 695, 2021.

Østrem, G.: Ice melting under a thin layer of moraine, and the existence of ice cores in moraine ridges, Geografiska Annaler, 41, 228–230, https://doi.org/10.1080/20014422.1959.11907953, 1959.

Petersen, E., Hock, R., Fochesatto, G. J., and Anderson, L. S.: The Significance of Convection in Supraglacial Debris Revealed Through
435   Novel Analysis of Thermistor Profiles, Journal of Geophysical Research: Earth Surface, 127, e2021JF006 520, 2022.

Quincey, D. J. and Glasser, N. F.: Morphological and ice-dynamical changes on the Tasman Glacier, New Zealand, 1990–2007, Global and Planetary Change, 68, 185–197, https://doi.org/10.1016/j.gloplacha.2009.05.003, 2009.

Reid, T. D. and Brock, B. W.: An energy-balance model for debris-covered glaciers including heat conduction through the debris layer, Journal of Glaciology, 56, 903–916, https://doi.org/10.3189/002214310794457218, 2010.

440   Reznichenko, N., Davies, T., Shulmeister, J., and McSaveney, M.: Effects of debris on ice-surface melting rates: an experimental study, Journal of Glaciology, 56, 384–394, https://doi.org/10.3189/002214310792447725, 2010.

Rounce, D., Quincey, D., and McKinney, D.: Debris-covered glacier energy balance model for Imja–Lhotse Shar Glacier in the Everest region of Nepal, The Cryosphere, 9, 2295–2310, https://doi.org/doi.org/10.5194/tc-9-2295-2015, 2015.

Rowan, A. V., Egholm, D. L., Quincey, D. J., and Glasser, N. F.: Modelling the feedbacks between mass balance, ice flow and debris transport
445   to predict the response to climate change of debris-covered glaciers in the Himalaya, Earth and Planetary Science Letters, 430, 427–438, 2015.

Rowan, A. V., Nicholson, L. I., Quincey, D. J., Gibson, M. J., Irvine-Fynn, T. D., Watson, C. S., Wagnon, P., Rounce, D. R., Thompson, S. S., Porter, P. R., et al.: Seasonally stable temperature gradients through supraglacial debris in the Everest region of Nepal, Central Himalaya, Journal of Glaciology, 67, 170–181, https://doi.org/10.1017/jog.2020.100, 2021.

450   Salazar, A.: On thermal diffusivity, European Journal of Physics, 24, 351, https://doi.org/10.1088/0143-0807/24/4/353, 2003.

Scherler, D., Wulf, H., and Gorelick, N.: Global assessment of supraglacial debris-cover extents, Geophysical Research Letters, 45, 11–798, https://doi.org/10.1029/2018GL080158, 2018.

Shah, S. S., Banerjee, A., Nainwal, H. C., and Shankar, R.: Estimation of the total sub-debris ablation from point-scale ablation data on a debris-covered glacier, Journal of Glaciology, 65, 759–769, https://doi.org/10.1017/jog.2019.48, 2019.

455   Shugar, D. H. and Clague, J. J.: The sedimentology and geomorphology of rock avalanche deposits on glaciers, Sedimentology, 58, 1762–1783, https://doi.org/10.1111/j.1365-3091.2011.01238.x, 2011.

Strikwerda, J. C.: Finite difference schemes and partial differential equations, SIAM, https://doi.org/doi.org/10.1137/1.9780898717938, 2004.

Sundqvist, H. and Veronis, G.: A simple finite-difference grid with non-constant intervals, Tellus, 22, 26–31,
460   https://doi.org/doi.org/10.1111/j.2153-3490.1970.tb01933.x, 1970.

Thakuri, S., Salerno, F., Smiraglia, C., Bolch, T., D'Agata, C., Viviano, G., and Tartari, G.: Tracing glacier changes since the 1960s on the south slope of Mt. Everest (central Southern Himalaya) using optical satellite imagery, The Cryosphere, 8, 1297–1315, https://doi.org/10.5194/tc-8-1297-2014, 2014.

Thomas, J. W.: Numerical partial differential equations: finite difference methods, Springer Science & Business Media, 2013.

465 Tielidze, L. G., Bolch, T., Wheate, R. D., Kutuzov, S. S., Lavrentiev, I. I., and Zemp, M.: Supra-glacial debris cover changes in the Greater Caucasus from 1986 to 2014, The Cryosphere, 14, 585–598, https://doi.org/10.5194/tc-14-585-2020, 2020.

Weisberg, S.: Applied linear regression, vol. 528, John Wiley & Sons, 2005.

Zhang, T. and Osterkamp, T.: Considerations in determining thermal diffusivity from temperature time series using finite difference methods, Cold Regions Science and Technology, 23, 333–341, https://doi.org/doi.org/10.1016/0165-232X(94)00021-O, 1995.